Supporting Information

Insight into role of side chains on the microstructure and carrier mobility in high-performance conjugated polymers

Yuchai Pan,[‡a,b] Jianyao Huang,[‡a] Dong Gao,[a] Zhihui Chen,[a] Weifeng Zhang[a] and Gui Yu*[a,b]

[a] Beijing National Laboratory for Molecular Sciences, CAS Research/Education Center for Excellence in Molecular Sciences, Institute of Chemistry, Chinese Academy of Sciences, Beijing 100190, China.

[b] School of Chemical Sciences, University of Chinese Academy of Sciences, Beijing 100049, China

Supporting Information

Contents:

1. General methods and synthesis

2. Gel permeation chromatography

3. Differential scanning calorimetry

4. Theoretical calculation

5. Cyclic voltammetry

6. Field-effect properties

7. Atomic force microscopy images

8. GIWAXS data and simulation

9. NMR spectra of new compounds and polymers

1. General methods and synthesis

Instruments and Characterization Conditions.

Materials. The reagents and starting materials were commercially available and used without any further purification otherwise indicated. Anhydrous THF was purified with a standard distillation procedure before use.

Nuclear Magnetic Resonance (NMR). ^{1}H NMR and ^{13}C NMR spectra at 298 K were recorded on a Bruker DMX 300 spectrometer. ^{1}H NMR spectra of polymers at 373 K were recorded on a Bruker Avance III 500 spectrometer. Chemical shifts are reported as δ values [ppm] relative to internal tetramethylsilane (TMS).

Mass spectroscopy. MALDI-TOF mass spectra were collected on an Autoflex III (Bruker Daltonics Inc.) MALDI-TOF spectrometer.

Gel permeation chromatography (GPC). Molecular weights were measured by GPC at 150 °C on a PL-220 system using 1,2,4-trichlorobenzene as eluent.

Thermogravimetric analyses (TGA). TGA profiles were recorded on a PerkinElmer TGA-8000 thermal analysis system at a heating rate of 10 °C min^{-1} under a nitrogen atmosphere.

Differential scanning calorimetry (DSC). DSC analyses were conducted on a TA Instrument DSC250 calorimeter. Two heating cycles were tested for each polymer sample. The second cycle DSC scan was recorded for analysis.

UV-vis absorption. UV-vis absorption spectra were recorded on a Hitachi UH4150 spectrophotometer. The concentrations of the polymer solutions were approximately 0.01 mg/mL. The thin films for absorption measurements were coated from 1 mg/mL solution onto quartz.

Cyclic voltammetry. Cyclic voltametric measurements were conducted on a CHI660c electrochemical workstation with a three-electrode-cell structure. A solution of 0.1 M tetrabutylammonium hexylfluorophosphate in anhydrous acetonitrile was used as the electrolyte. A Ag/AgCl (Ag in a 0.01 mol L^{-1} KCl) electrode and a platinum wire were used as the reference electrode and the counter electrode, respectively. A glassy carbon stick electrode coated with a polymer was used as the working electrode. All the cyclic voltametric traces were calibrated by the ferrocenium/ferrocene (Fc$^+$/Fc) couple (4.80 eV below the vacuum level).

Atomic force microscopy. AFM images were collected using Bruker Multimode 8 atomic force microscope in ScanAsyst mode.

Grazing-incidence wide-angle X-ray scattering (GIWAXS). GIWAXS data were collected at BL14B1 Station of Shanghai Synchrotron Radiation Facility (SSRF) with a beam energy of 11.0 keV (λ = 1.1271 Å) and an incident angle of 0.2°. The GIWAXS patterns were calibrated using a standard lanthanum boride sample. 1D cross-sectional data was integrated using the software FIT2D.[1] The coherence length $L_c = 2\pi K/\Delta q_{hkl}$, where K is the Scherrer constant and Δq_{hkl} is the full width at half-maximum of the diffraction peak with regard to the scattering vector q.[2]

Calculation

DFT calculations were performed using the Gaussian 09 package.[3] MM/MD calculations were conducted using the Materials Studio package with the Dreiding force field. Unit cells containing a co-repeating unit was built with different cell parameters using the periodic boundary condition. 200 ps-quenched dynamics (NPT, quench frequency = 1 ps) were performed on each structure at 400 K to afford the stable structures.

Monomer Synthesis

(*E*)-1,2-bis(3-*n*-alkyl-thieno[3,2-*b*]thiophen-2-yl)ethene monomers were prepared according to previously reported procedures within 5 steps.[4]

General procedure. (*E*)-1,2-bis(3-*n*-alkyl-thieno[3,2-*b*]thiophen-2-yl)ethene (2 mmol) was added to a solution of anhydrous THF under N_2 atmosphere and the system was cooled to −78 °C. Then *n*-BuLi (2.5 M in hexane, 1.67 mL, 4.18 mmol) was added dropwise to the solution and the suspension was stirred at −30 °C for 2 h. Then a 1.0 M solution of Me_3SnCl (1.0 M in hexane, 8.2 mL, 8.2 mmol) in THF was added in a batch at −78 °C. The mixture was stirred at −30 °C for another 5 h. The mixture was then quenched with water, extracted with petroleum ether, and washed with brine. The combined organic extracts were dried over anhydrous Na_2SO_4 and the solvent was removed. The obtained crude solid was purified by recrystallization from dichloromethane and methanol to yield the ditin monomer as a yellow to orange solid.

(*E*)-1,2-bis(5-(trimethylstannyl)-3-*n*-octyl-thieno[3,2-*b*]thiophen-2-yl)ethene. Yield: 1.26 g, 73.6%. ¹H NMR (300 MHz, CD_2Cl_2): δ (ppm) 7.24 (s, 2H), 7.08 (s, 2H), 2.82 (t, *J* = 7.5 Hz, 4H), 1.73 (m, 4H), 1.36-1.27 (br, 20H), 0.88 (t, *J* = 7.5 Hz, 6H), 0.41 (t, *J* = 30 Hz, 18H). ¹³C NMR (75 MHz, CD_2Cl_2): δ: 147.48, 142.02, 138.70, 137.91, 132.93, 127.33, 120.20, 29.82, 29.76, 29.69, 29.64, 28.66, 23.09, 14.29, −8.12. HR-MS (MALDI-TOF) m/z: Anal. Calc. for $C_{36}H_{56}S_4Sn_2$: 856.130837. Found: 856.131088.

(*E*)-1,2-bis(5-(trimethylstannyl)-3-*n*-nonyl-thieno[3,2-*b*]thiophen-2-yl)ethene. Yield: 1.44 g, 81.4%.¹H NMR (300 MHz, CD_2Cl_2): δ (ppm) 7.24 (s, 2H), 7.08 (s, 2H), 2.83 (t, *J* = 7.5 Hz, 4H), 1.74 (m, 4H), 1.38-1.25 (br, 24H), 0.87 (t, *J* = 7.5 Hz, 6H), 0.42 (t, *J* = 30 Hz, 18H). ¹³C NMR (75 MHz, CD_2Cl_2): δ: 147.56,

142.04, 138.79, 137.99, 132.98, 127.37, 120.31, 32.36, 29.98, 29.85, 29.84, 29.79, 29.73, 28.71, 23.14, 14.32, −8.09. HR-MS (MALDI-TOF) m/z: Anal. Calc. for $C_{38}H_{60}S_4Sn_2$: 884.162213. Found: 884.162221.

(*E*)-1,2-bis(5-(trimethylstannyl)-3-*n*-decyl-thieno[3,2-*b*]thiophen-2-yl)ethene. Yield: 1.41 g, 77.3%. ^{1}H NMR (300 MHz, CD$_2$Cl$_2$): δ (ppm) 7.24 (s, 2H), 7.08 (s, 2H), 2.82 (t, *J* = 7.5 Hz, 4H), 1.73 (m, 4H), 1.38-1.24 (m, 28H), 0.88 (t, *J* = 7.5 Hz, 6H), 0.41 (t, *J* = 30 Hz, 18H). ^{13}C NMR (101 MHz, CD$_2$Cl$_2$): δ: ^{13}C NMR (75 MHz, CD2Cl2) δ 147.49, 142.00, 138.73, 137.92, 132.93, 127.34, 120.22, 32.35, 30.06, 30.00, 29.79, 29.77, 29.68, 28.64, 23.11, 14.31, −8.12. HR-MS (MALDI-TOF) m/z: Anal. Calc. for $C_{40}H_{64}S_4Sn_2$: 912.193590. Found: 912.193227.

(*E*)-1,2-bis(5-(trimethylstannyl)-3-*n*-undecyl-thieno[3,2-*b*]thiophen-2-yl)ethene. Yield: 1.30 g, 69.3%. ^{1}H NMR (300 MHz, CD$_2$Cl$_2$): δ (ppm) 7.24 (s, 2H), 7.08 (s, 2H), 2.82 (t, *J* = 7.5 Hz, 4H), 1.74 (m, 4H), 1.38-1.26 (m, 32H), 0.88 (t, *J* = 7.5 Hz, 6H), 0.41 (t, *J* = 30 Hz, 18H). ^{13}C NMR (75 MHz, CD$_2$Cl$_2$): δ: 147.53, 142.01, 138.77, 137.96, 132.95, 127.36, 120.26, 32.37, 30.13, 30.09, 30.02, 29.81, 29.70, 28.67, 23.14, 14.33, −8.10. HR-MS (MALDI-TOF) m/z: Anal. Calc. for $C_{42}H_{68}S_4Sn_2$: 938.22419. Found: 938.224637.

2. Gel permeation chromatography
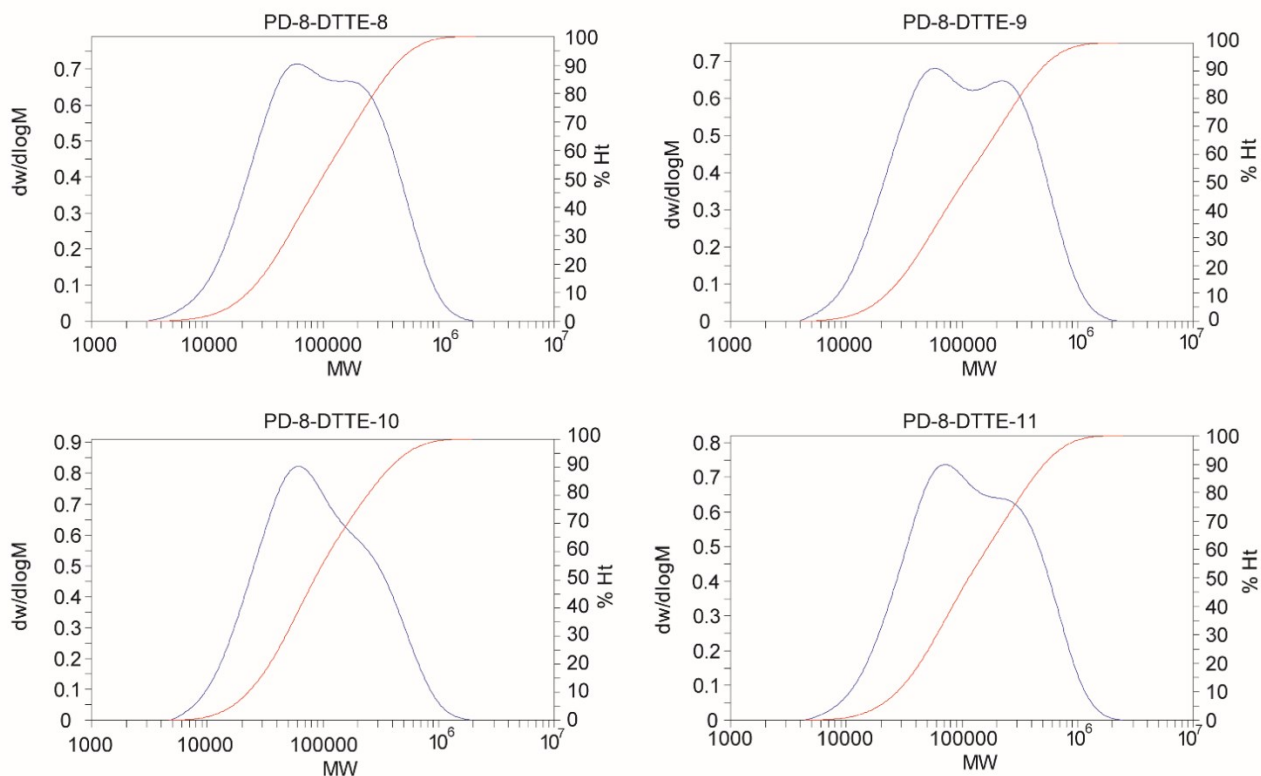
Fig S1 GPC plots of the polymers PD-8-DTTE-n (n = 8 to 11).

3. Differential scanning calorimetry
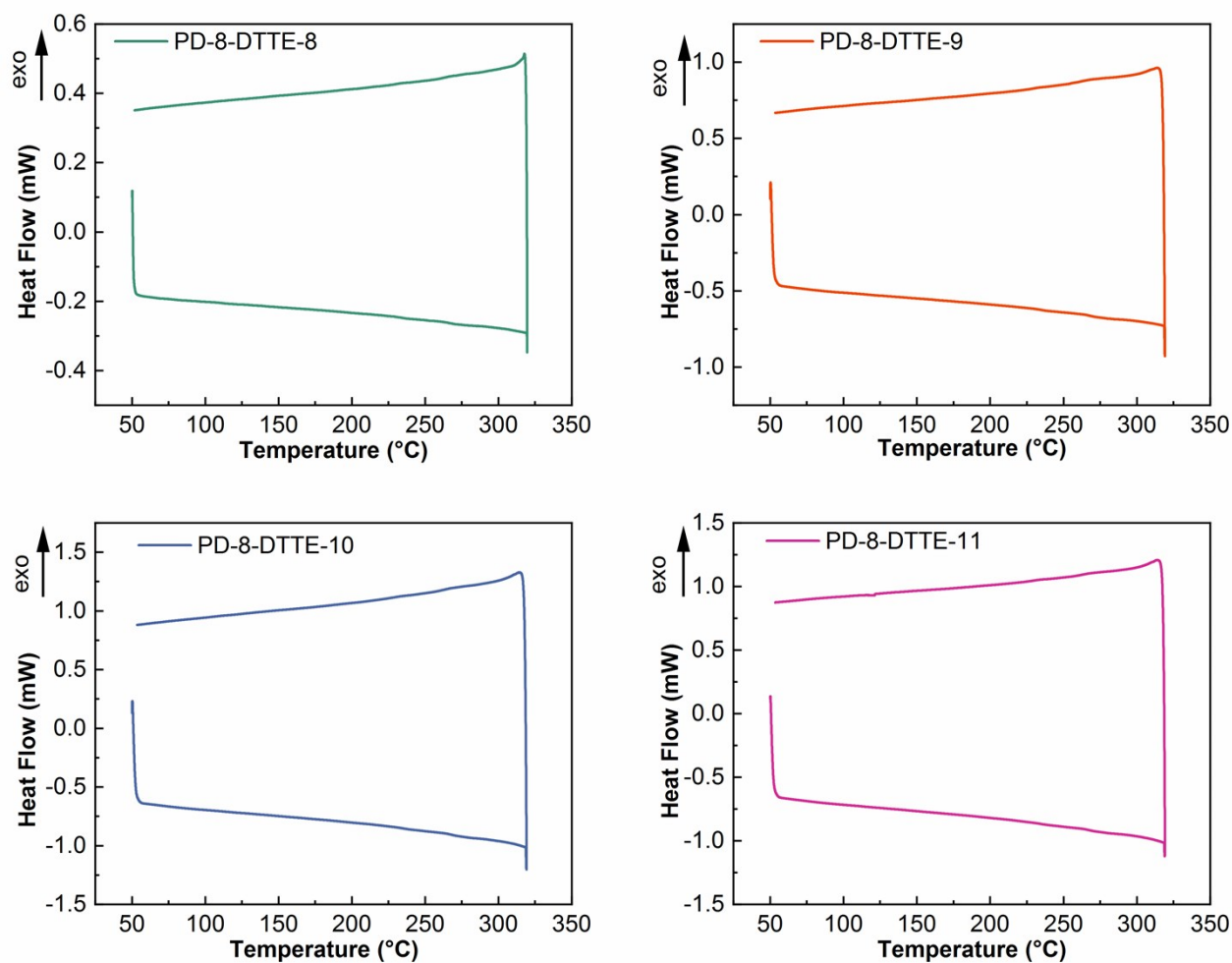
Fig. S2 Differential scanning calorimetry plots of the PD-8-DTTE-n (n = 8 to 11) films.
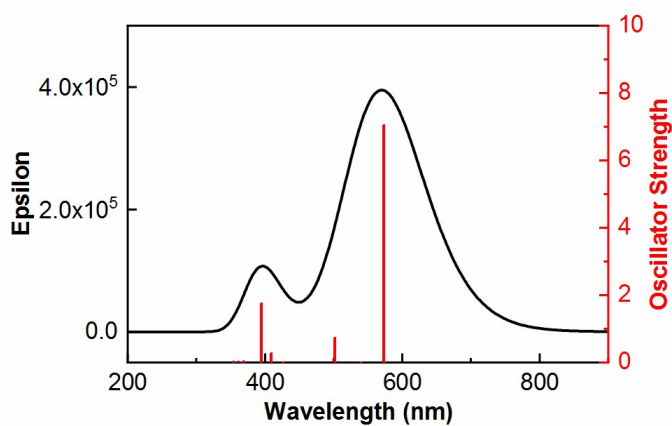
4. Theoretical Calculation

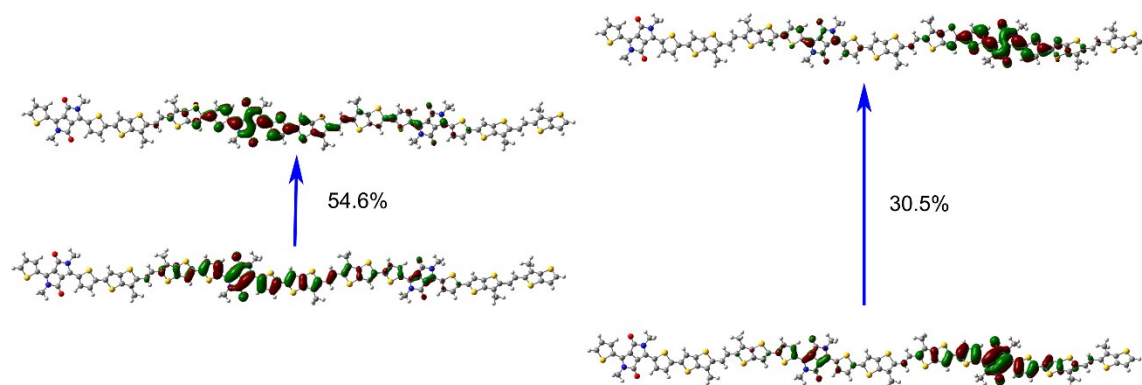**Fig S3** Calculated UV–visible absorption spectrum of the DPP–DTTE trimer at the CAM-B3LYP/6-31G(d) level.

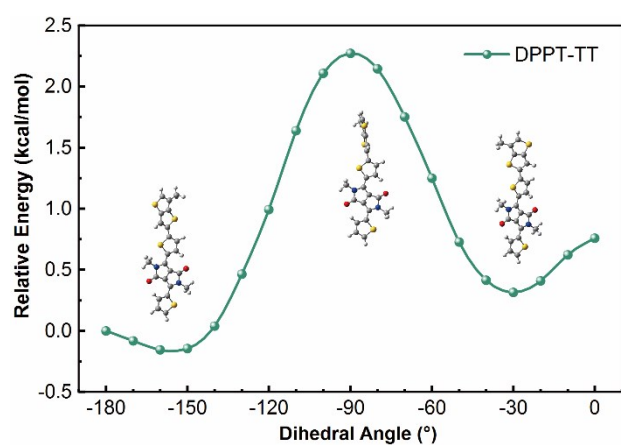**Fig S4** Major contribution of the $S_0 \rightarrow S_1$ natural transition orbital.

Fig. S5 Potential energy scan of the DPP-alkylated thienothiophene subunit.

Because the thiophene-flanked DPP has intramolecular hydrogen bonds that restrict the conformational change, the rotational disorder of the PD-DTTE backbone is mainly related to the thiophene–thienothiophene subunit. We performed potential energy scan at the ω97XD/6-31G(d) level of theory. Akin to the result reported in oligothiophene analogs, the thiophene–thienothiophene subunit prefers an *S*-trans conformation with a moderate rotational barrier. Two local thermodynamically stable conformers have dihedral angles of 20–30° between the dithienyl DPP and thienothiophene subunits. According to the small energy difference between the *S*-trans and *S*-cis conformers (0.47 kcal/mol), we predict that both conformers are present in the backbone.

5. Cyclic voltammetry
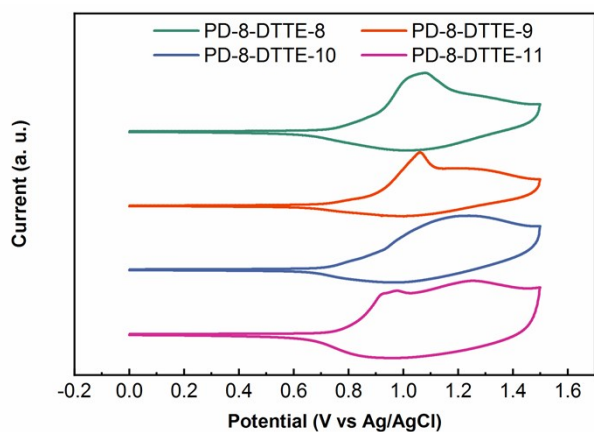
Fig. S6 Cyclic voltammetry traces of the polymers PD-8-DTTE-n (n = 8 to 11).

6. Field-effect properties
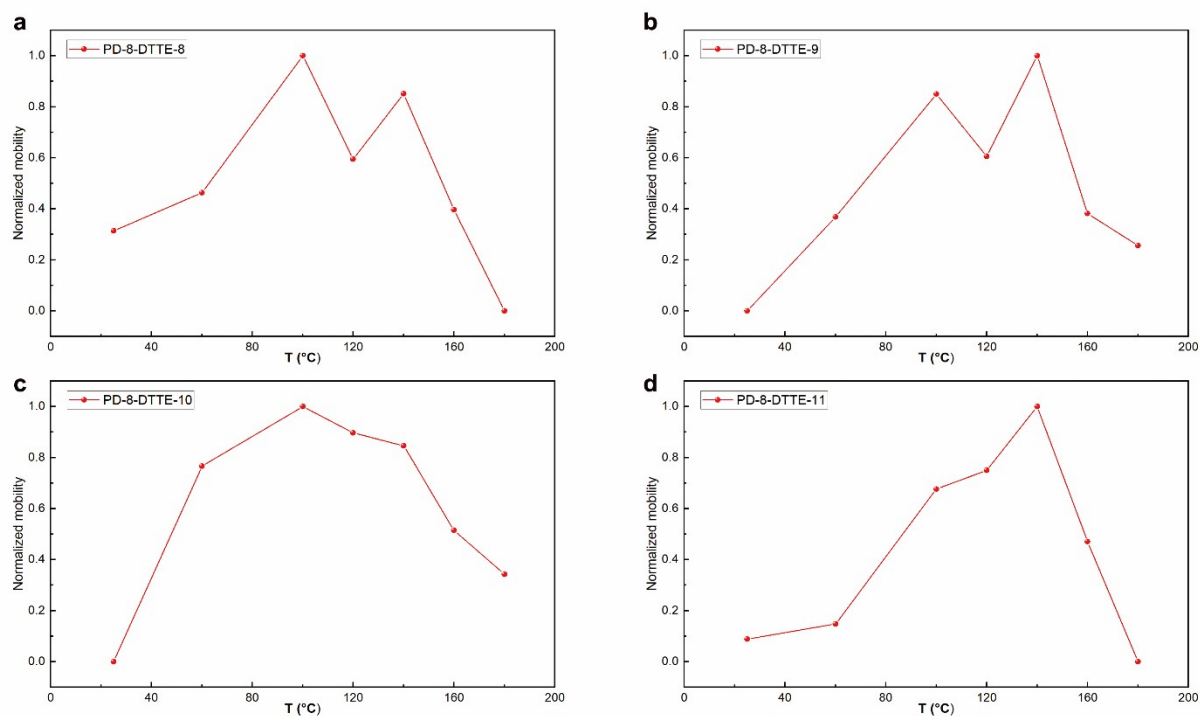
Fig. S7 Annealing temperature dependence of normalized mobilities for (a) PD-8-DTTE-8, (b) PD-8-DTTE-9, (c) PD-8-DTTE-10, and (d) PD-8-DTTE-11.
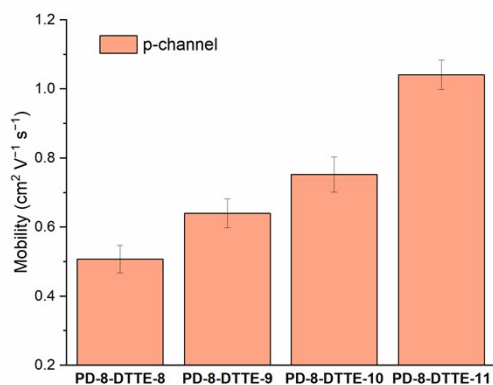
Fig. S8 Average saturation hole mobilities of PD-8-DTTE-n based thin-film transistors. Each value was obtained from more than 8 devices.
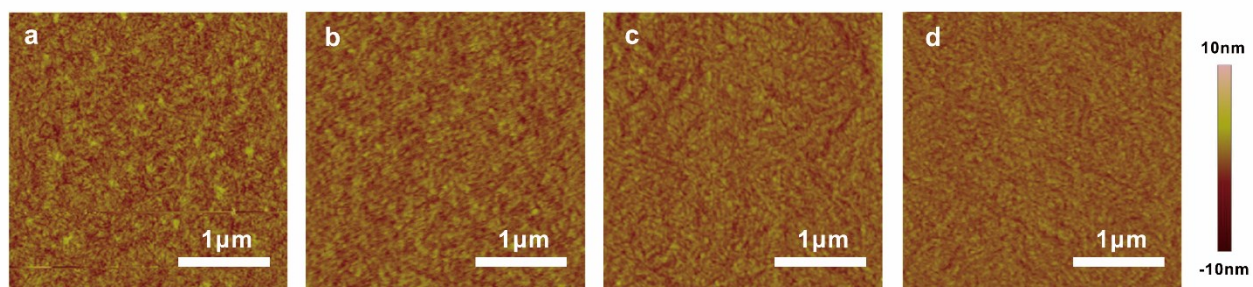
7. Atomic force microscopy images

Fig. S9 AFM images of as-spun PD-8-DTTE-n thin films: (a) PD-8-DTTE-8, (b) PD-8-DTTE-9, (c) PD-8-DTTE-10, and (d) PD-8-DTTE-11.

Table S1 Root-mean-square roughness of PD-8-DTTE-n (n = 8 to 11) thin films

Polymer	Root-mean-square roughness (nm)	
	As-spun	Annealed
PD-8-DTTE-8	1.21	1.15
PD-8-DTTE-9	0.93	1.01
PD-8-DTTE-10	0.82	0.88
PD-8-DTTE-11	0.72	0.82

8. GIWAXS data and simulation
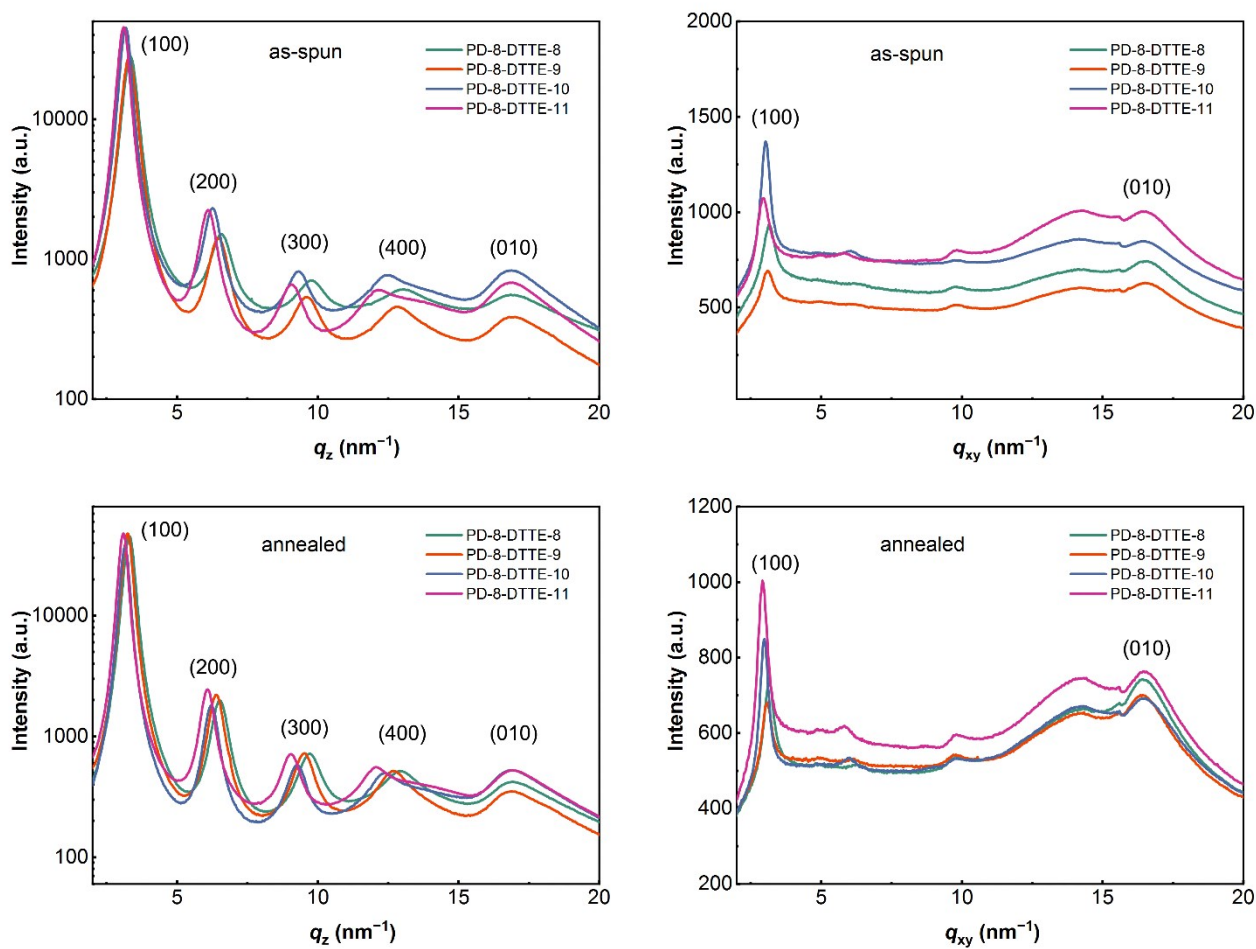
Fig. S10 1D cross-sectional profiles of GIWAXS pattern.
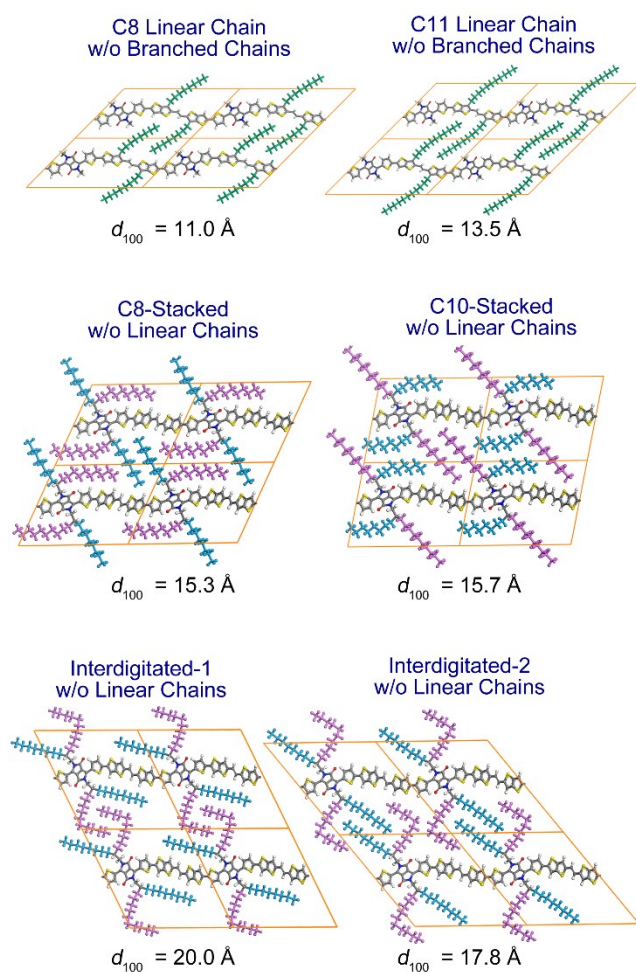
Fig. S11 Simulated crystal structure of monoalkylated PD-8-DTTE-8.

If only linear chains remain with removal of branched chains, the d-spacing depends largely on the length of linear chains (in this case, from octyl to undecyl) and is much shorter than the corresponding experimental result. By contrast, if linear side chains are removed, interdigitated and non-interdigitated packing motifs are both possible: the d-spacing of the interdigitated packing is comparable to the experiment, whereas the non-interdigitated open-arm structure has a much shorter lamellar distance (Fig. S14).
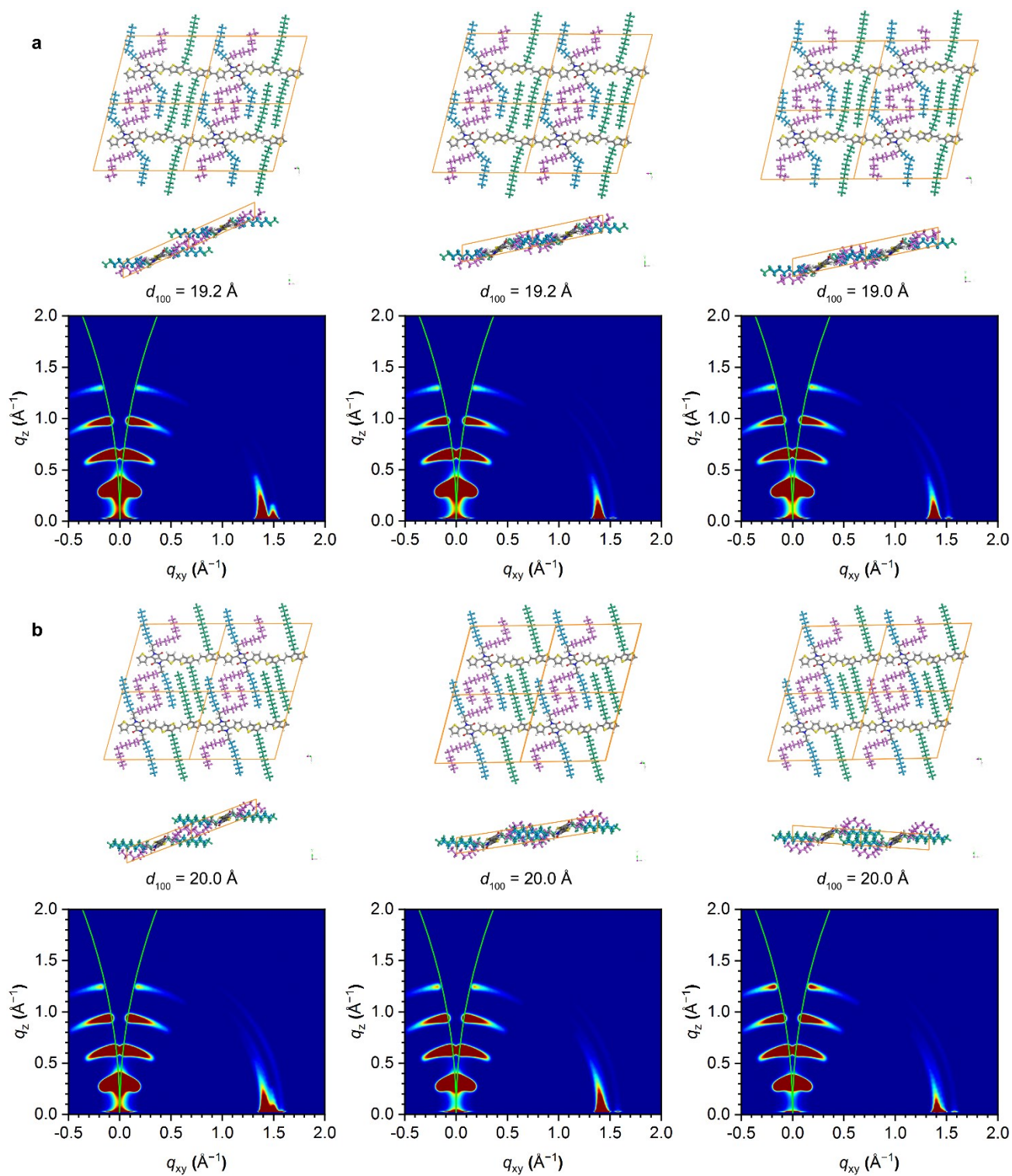
Fig. S12 Simulated thin-film GIWAXS patterns of (a) *anti*–C8–C11 and (b) *syn*–C8–C11. Three different polymorphs with different alkyl stackings (side view) are shown to describe the stacking motif. Green line is the Ewald contour (λ = 1.1271 Å and $\theta_{incidence}$ = 0.2°).
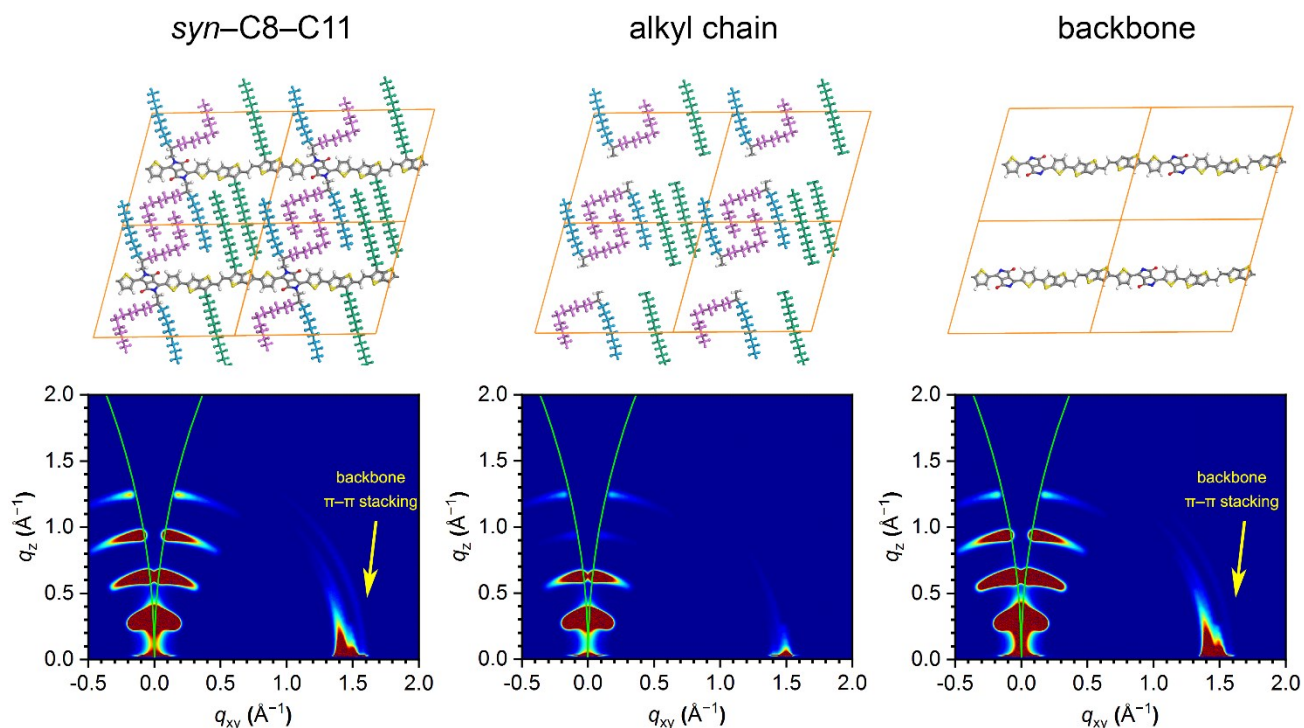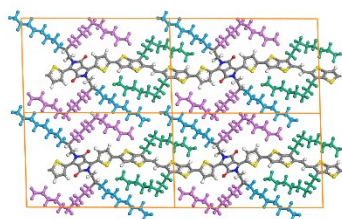
Fig. S13 Simulated thin-film GIWAXS patterns of the *syn*–C8–C11, extracted alkyl-chain and backbone stacking. Green line is the Ewald contour (λ = 1.1271 Å and $\theta_{incidence}$ = 0.2°).

We simulated the polycrystalline thin-film GIWAXS pattern to illustrate the different contribution of side chain and backbone. Take the *syn*-C8–C11 motif as an example. The simulation was completed using the software SimDiffraction.[5] The (100) axis was set to the preferred out-of-plane orientation with tilt angles in the range of −30° to 30°. Lorentz correction, polarization factor, Yoneda correction and structure factor correction were used in the simulation. Scattering peaks up to (400) and (010) were simulated. The simulated results indicate that various polymorphs of a give stacking motif have limited influences on the microstructural parameters. The π-stacking scattering peak differs in different motifs. The *syn*-C8–C11 motif has a smaller π-stacking distance compared with that of the *anti*-C8–C11 motif. Alkyl-chain packing and backbone stacking both contribute to the scattering pattern. We found that backbone π–π stacking led to a peak at ca. 1.6 Å^{-1} in the simulated *syn*-C8–C11 pattern. This result typically reflects the experimental pattern.

Noninterdigitated PD-8-DTTE-8

a = 17.509128 Å
b = 4.945236 Å
c = 26.058837 Å
α = 100.78268°
β = 95.37866°
γ = 69.02585°
d_{100} = 16.3 Å

Interdigitated PD-8-DTTE-8
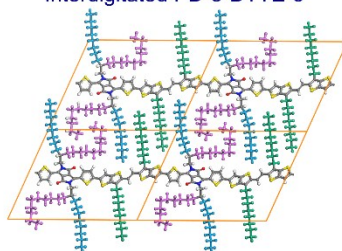
a = 20.811698 Å
b = 4.738299 Å
c = 26.308379 Å
α = 106.5616°
β = 75.38196°
γ = 67.82525°
d_{100} = 17.6 Å

Fig. S14 Noninterdigitated and interdigitated patterns of simulated PD-8-DTTE-8 crystals.
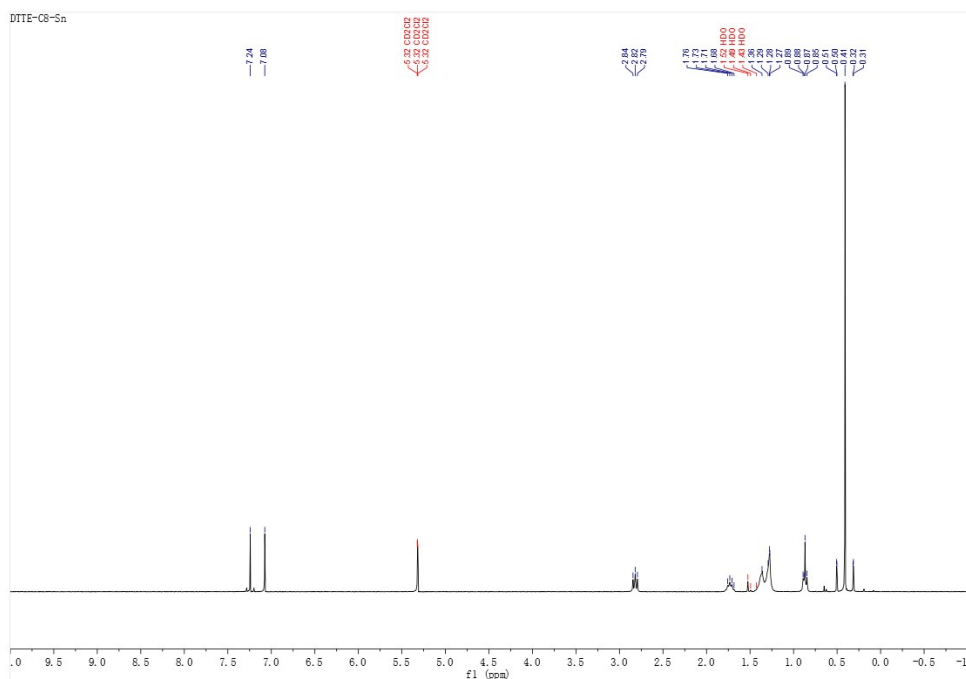
9. NMR spectra of new compounds

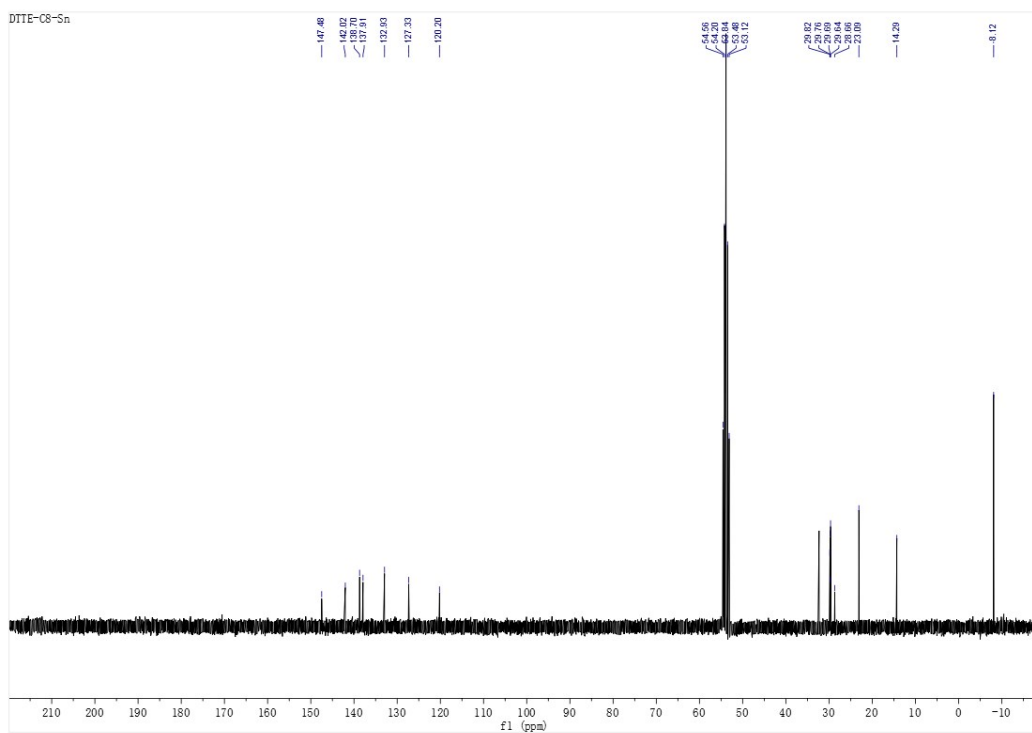**Fig. S15** ¹H NMR spectrum of (*E*)-1,2-bis(5-(trimethylstannyl)-3-*n*-octyl-thieno[3,2-*b*]thiophen-2-yl)ethene.

Fig. S16 ¹³C NMR spectrum of (*E*)-1,2-bis(5-(trimethylstannyl)-3-*n*-octyl-thieno[3,2-*b*]thiophen-2-yl)ethene.
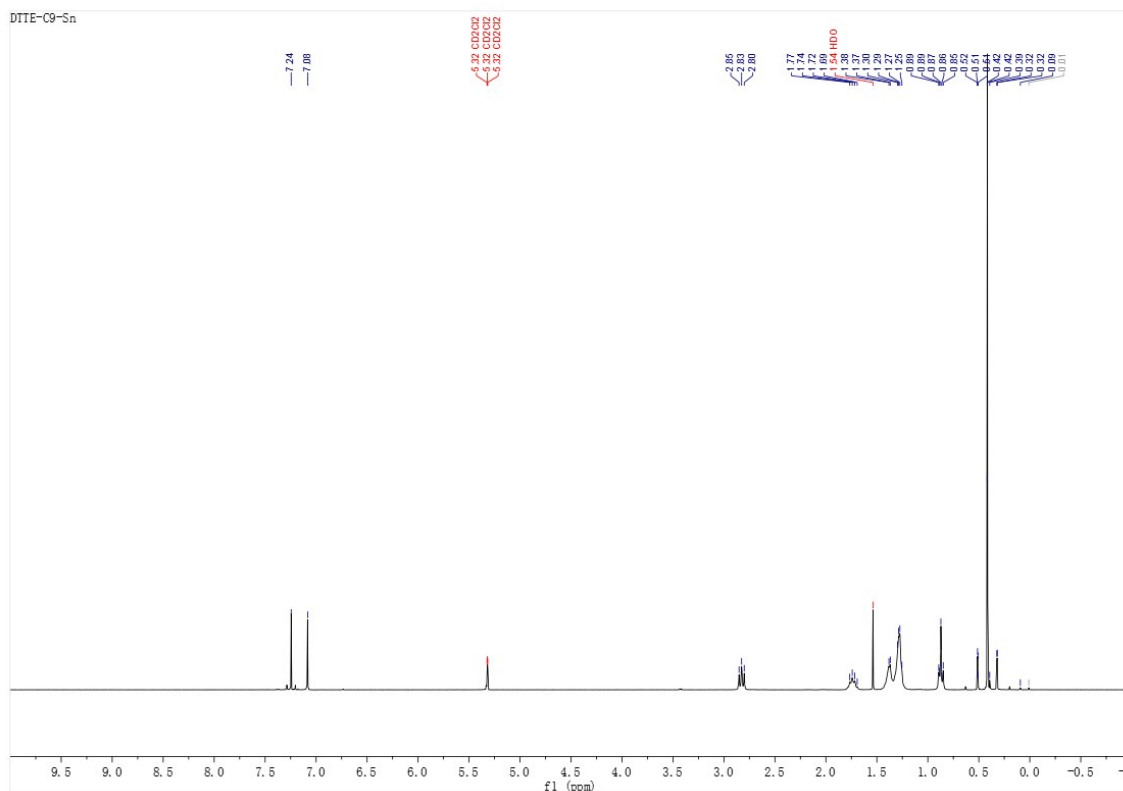
Fig. S17 ¹H NMR spectrum of (*E*)-1,2-bis(5-(trimethylstannyl)-3-*n*-nonyl-thieno[3,2-*b*]thiophen-2-yl)ethene.
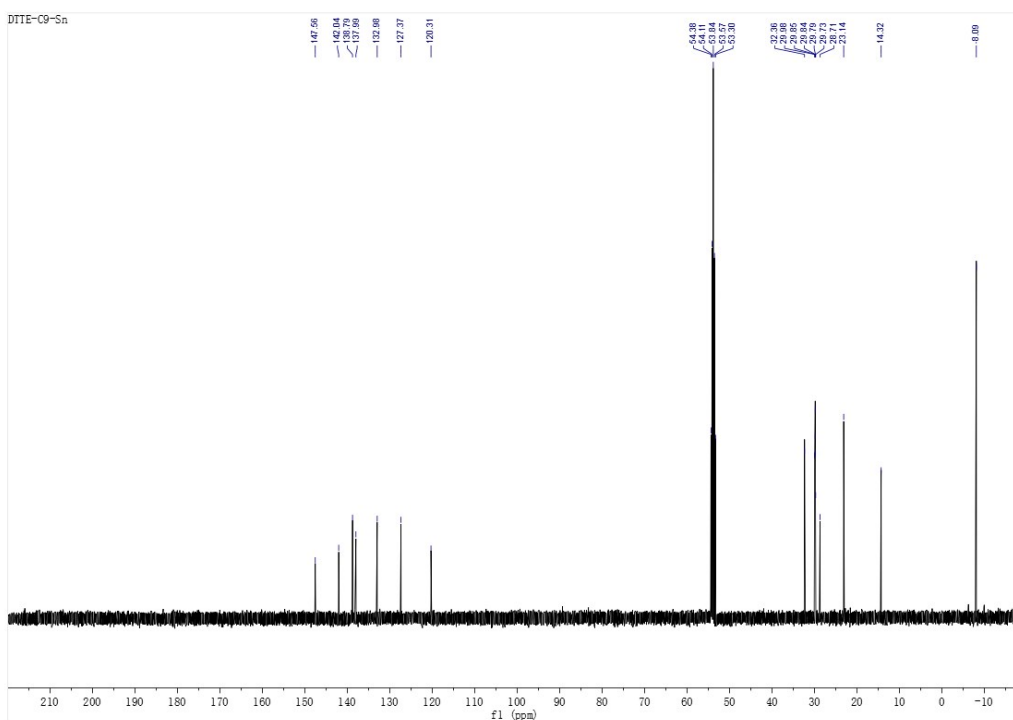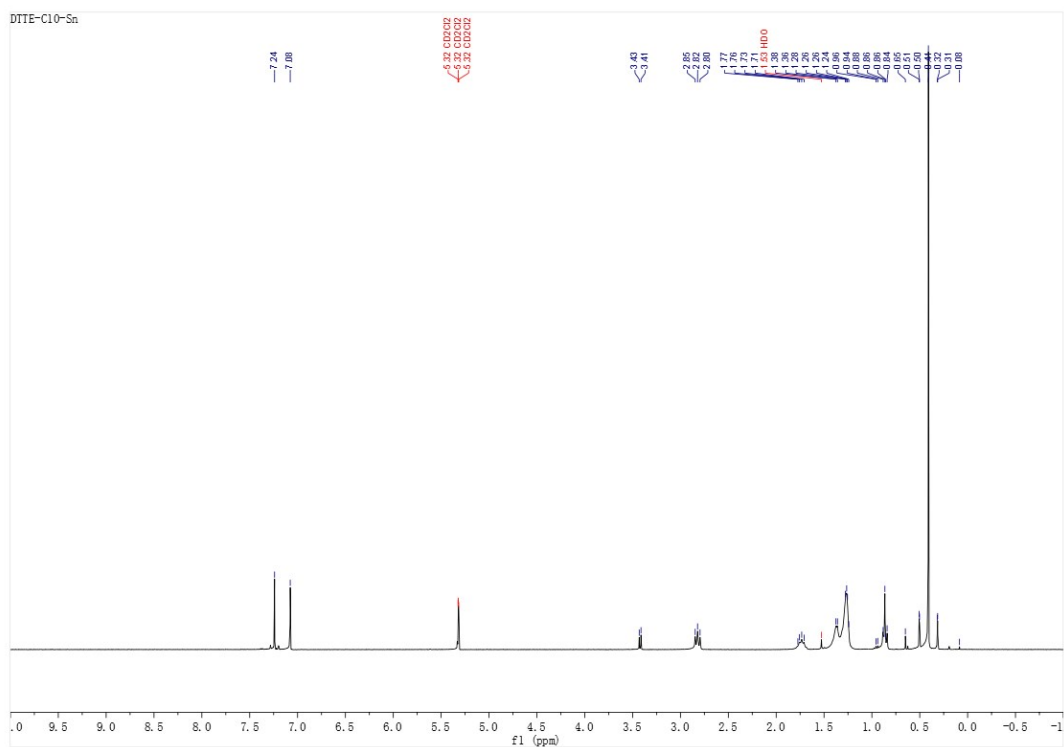

Fig. S18 ¹³C NMR spectrum of (*E*)-1,2-*bis*(5-(trimethylstannyl)-3-*n*-nonyl-thieno[3,2-*b*]thiophen-2-yl)ethene.

Fig. S19 ^{1}H NMR spectrum of (*E*)-1,2-bis(5-(trimethylstannyl)-3-*n*-decyl-thieno[3,2-*b*]thiophen-2-yl)ethene.
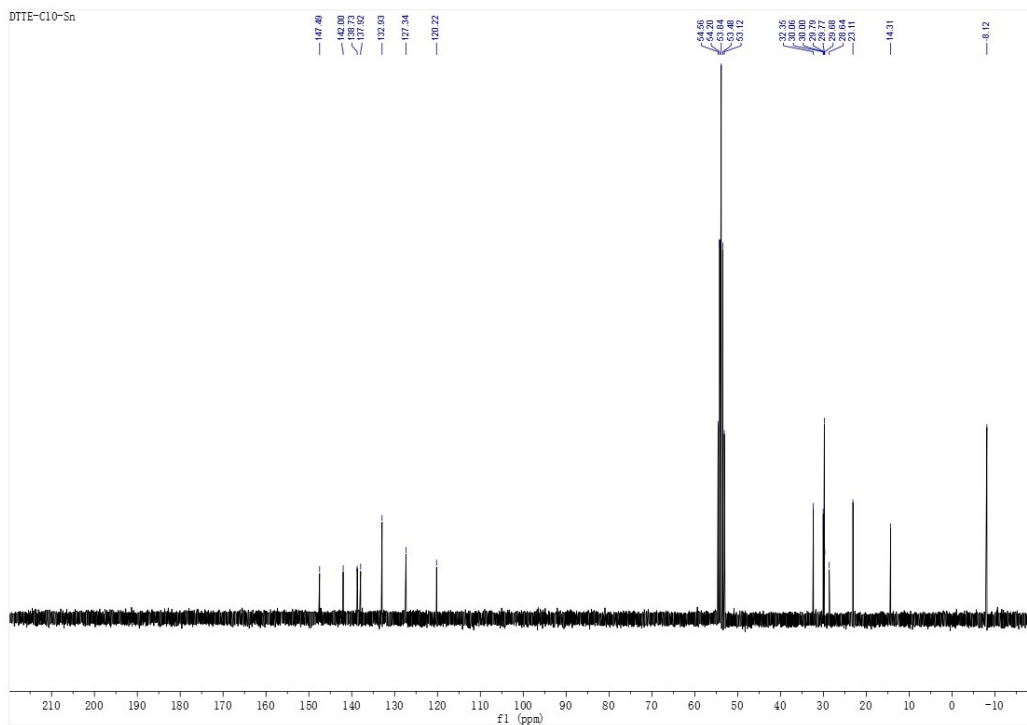

Fig. S20 ^{13}C NMR spectrum of (*E*)-1,2-bis(5-(trimethylstannyl)-3-*n*-decyl-thieno[3,2-*b*]thiophen-2-yl)ethene.
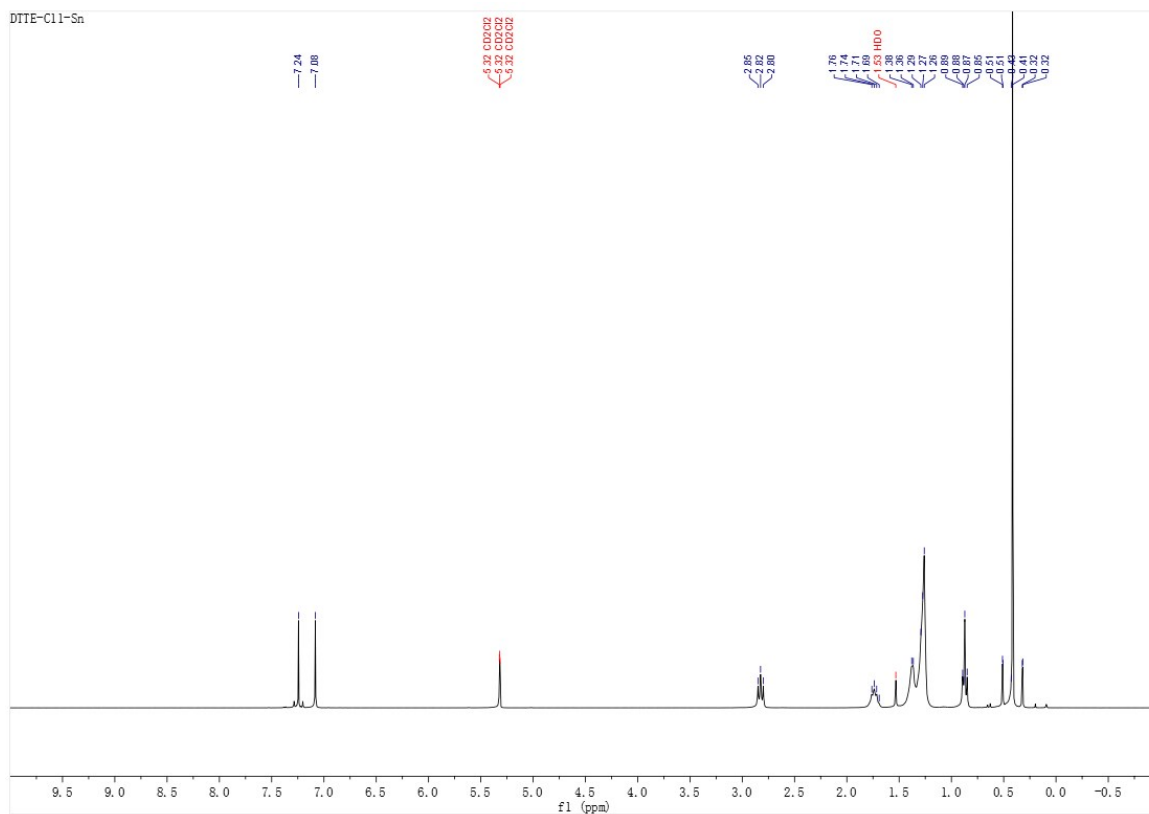
Fig. S21 ¹H NMR spectrum of (*E*)-1,2-bis(5-(trimethylstannyl)-3-*n*-undecyl-thieno[3,2-*b*]thiophen-2-yl)ethene.
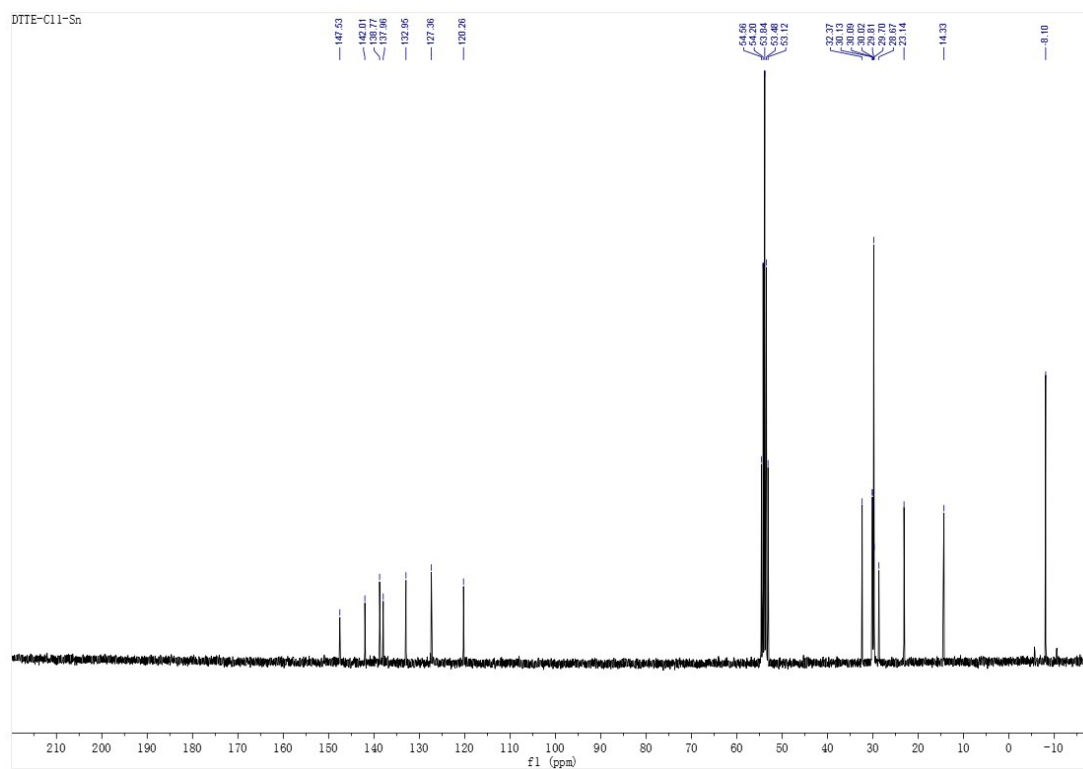

Fig. S22 ¹³C NMR spectrum of (*E*)-1,2-bis(5-(trimethylstannyl)-3-*n*-undecyl-thieno[3,2-*b*]thiophen-2-yl)ethene.
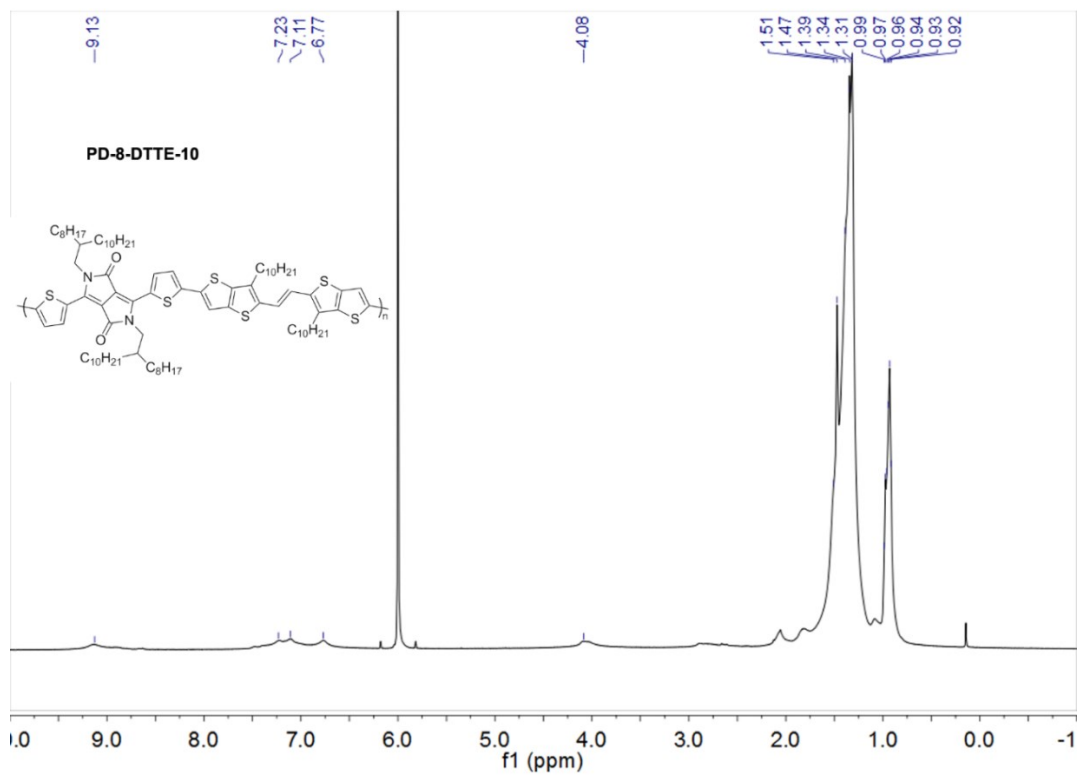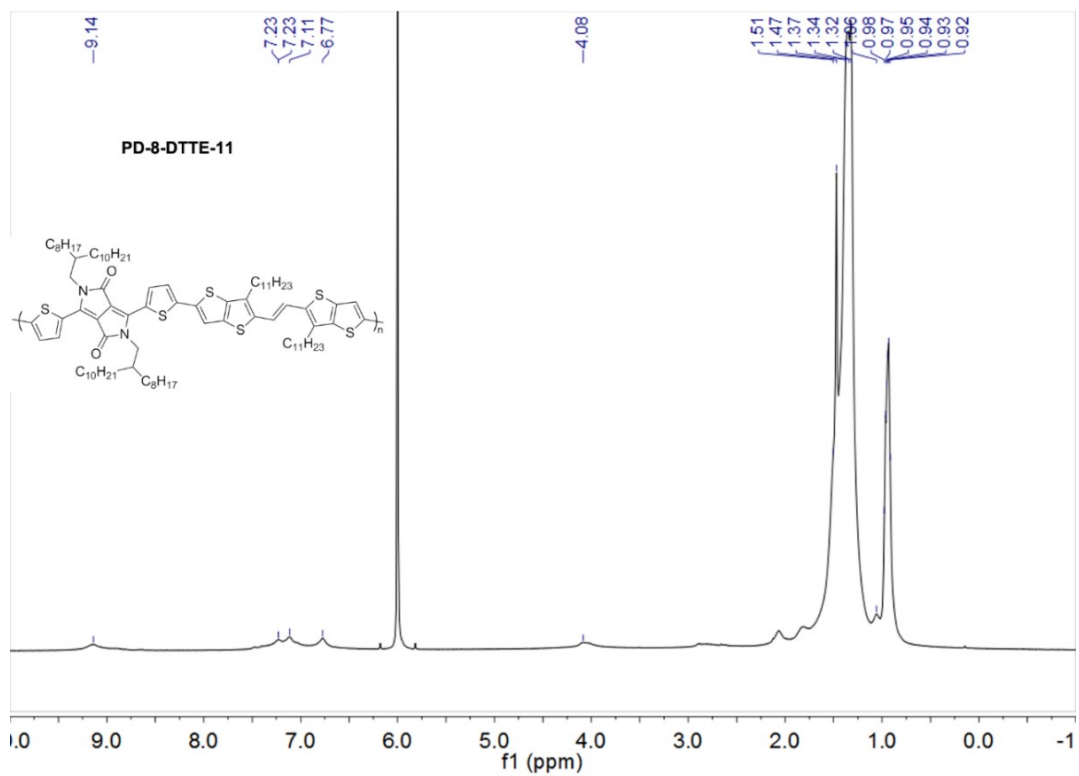
Fig. S23 ¹H NMR spectrum of the polymer PD-8-DTTE-8.

Fig. S24 ¹H NMR spectrum of the polymer PD-8-DTTE-9.

Fig. S25 ^{1}H NMR spectrum of the polymer PD-8-DTTE-10.

Fig. S26 ^{1}H NMR spectrum of the polymer PD-8-DTTE-11.

REFERENCES

1.   A. P. Hammersley, *J. Appl. Crystallogr.*, 2016, **49**, 646-652.

2.   D. M. Smilgies, *J. Appl. Crystallogr.*, 2009, **42**, 1030-1034.

3.   M. J. Frisch, G. W. Trucks, H. B. Schlegel, G. E. Scuseria, M. A. Robb, J. R. Cheeseman, G. Scalmani, V. Barone, B. Mennucci, G. A. Petersson, H. Nakatsuji, M. Caricato, X. Li, H. P. Hratchian, A. F. Izmaylov, J. Bloino, G. Zheng, J. L. Sonnenberg, M. Hada, M. Ehara, K. Toyota, R. Fukuda, J. Hasegawa, M. Ishida, T. Nakajima, Y. Honda, O. Kitao, H. Nakai, T. Vreven, J. A. Montgomery, J. E. Peralta, F. Ogliaro, M. Bearpark, J. J. Heyd, E. Brothers, K. N. Kudin, V. N. Staroverov, R. Kobayashi, J. Normand, K. Raghavachari, A. Rendell, J. C. Burant, S. S. Iyengar, J. Tomasi, M. Cossi, N. Rega, J. M. Millam, M. Klene, J. E. Knox, J. B. Cross, V. Bakken, C. Adamo, J. Jaramillo, R. Gomperts, R. E. Stratmann, O. Yazyev, A. J. Austin, R. Cammi, C. Pomelli, J. W. Ochterski, R. L. Martin, K. Morokuma, V. G. Zakrzewski, G. A. Voth, P. Salvador, J. J. Dannenberg, S. Dapprich, A. D. Daniels, Ö. Farkas, J. B. Foresman, J. V. Ortiz, J. Cioslowski and D. J. Fox,   *Gaussian 09*, 2009.

4.   a) X. Zhang, M. Köhler and A. J. Matzger, *Macromolecules*, 2004, **37**, 6306-6315; b) D. Gao, K. Tian, W. Zhang, J. Huang, Z. Chen, Z. Mao and G. Yu, *Polym. Chem.*, 2016, **7**, 4046-4053.

5.   D. W. Breiby, O. Bunk, J. W. Andreasen, H. T. Lemke and M. M. Nielsen, *J. Appl. Crystallogr.*, 2008, **41**, 262-271.